Short title: Affinity purification of plant mitochondria

Author for contact:

Andreas P.M. Weber, [1]Institute of Plant Biochemistry, Cluster of Excellence on Plant Science (CEPLAS), Heinrich Heine University, Universitätsstrasse 1, 40225 Düsseldorf, Germany

Rapid single-step affinity purification of HA-tagged mitochondria from *Arabidopsis thaliana*

Franziska Kuhnert[1], Anja Stefanski[2], Nina Overbeck[2], Kai Stühler[2], Andreas P.M. Weber[1]

[1]Institute of Plant Biochemistry, Cluster of Excellence on Plant Science (CEPLAS), Heinrich Heine University, Universitätsstrasse 1, 40225 Düsseldorf, Germany

[2]Molecular Proteomics Laboratory, Biomedical Research Center, Heinrich Heine University, Universitätsstrasse 1, 40225 Düsseldorf, Germany

One-sentence summary: Affinity-tagging of mitochondria in plant cells with a triple hemagglutinin-tag enables single-step affinity purification of mitochondria in less than 20 min.

Author contributions: F.K. generated transgenic lines harboring affinity-tagged mitochondria, isolated mitochondria, analyzed the data, and drafted the manuscript; A.S., N.O., and K.S. performed the proteomics analysis and analyzed the data; A.P.M.W. conceived and supervised the experiments and contributed to the writing of the manuscript.

Funding: This work was supported by the Deutsche Forschungsgemeinschaft (CRC 1208 and funding under Germany´s Excellence Strategy – EXC-2048/1 – project ID 390686111“).

29

30 **Email address of the author for contact:** aweber@hhu.de

ABSTRACT

Photosynthesis in plant cells would not be possible without the supportive role of mitochondria. However, isolation of mitochondria from plant cells, for physiological and biochemical analyses, is a lengthy and tedious process. Established isolation protocols require multiple centrifugation steps and substantial amounts of starting material. To overcome these limitations, we tagged mitochondria in *Arabidopsis thaliana* with a triple haemagglutinin-tag for rapid purification via a single affinity purification step. This protocol yields a substantial quantity of highly pure mitochondria from 1 g of Arabidopsis seedlings. The purified mitochondria were suitable for enzyme activity analyses and yielded sufficient amounts of proteins for deep proteomic profiling. We applied this method for the proteomic analysis of the Arabidopsis *bou-2* mutant deficient in the mitochondrial glutamate transporter À bout de souffle (BOU) and identified 27 differentially expressed mitochondrial proteins compared with transgenic Col-0 controls. Our work also sets the stage for the development of advanced mitochondria isolation protocols for distinct cell types.

INTRODUCTION

In all eukaryotic organisms, mitochondria are the major source of ATP, which is produced via the oxidative phosphorylation (OXPHOS) pathway, thus playing a vital role in cellular energy metabolism. Mitochondria also participate in amino acid metabolism as well as in photorespiration in photosynthetic eukaryotes. Photorespiration plays a crucial role in photosynthesis by detoxifying 2-phosphoglycolate, which is produced by the oxygenation of Rubisco and acts as an inhibitor of several plastidial enzymes (Ogren and Bowes, 1971; Kelly and Latzko, 1976; Husic et al., 1987). Plants reclaim 2-phosphoglycolate in the complex pathway of photorespiration, yielding 3-phosphoglycerate, which is returned to the Calvin Benson cycle. The photorespiratory pathway includes several enzymatic steps that occur in four subcellular compartments: plastids, peroxisomes, mitochondria, and cytosol (Eisenhut et al., 2019). Knockout mutants of genes encoding enzymes and transporters involved in photorespiration often show a photorespiratory phenotype, characterized by chlorotic leaves and growth inhibition under ambient carbon dioxide (CO_2) conditions, which can be rescued in a CO_2 enriched environment (Peterhansel et al., 2010). A key step in photorespiration is the conversion of two glycine molecules into one serine residue in the mitochondrial matrix, accompanied by the release of CO_2 and ammonia. This step is catalyzed by the glycine decarboxylase (GDC) multienzyme system, comprising a P-protein (GLDP), H-protein (GDCH), L-protein (GDCL), and T-protein (GLDT), in combination with serine hydroxymethyltransferase (SHM) (Voll et al., 2006; Engel et al., 2007). In green tissues, these proteins constitute up to 50% of the total protein content of the mitochondrial matrix, indicating the importance of glycine oxidation in mitochondria (Oliver et al., 1990).

The *Arabidopsis thaliana bou-2* mutant was previously identified as lacking the mitochondrial glutamate transporter À bout de souffle (BOU), which is involved in photorespiration (Eisenhut et al., 2013). Plants lacking the inner mitochondrial membrane (IMM) protein BOU show a pronounced photorespiratory phenotype under ambient CO_2 conditions, significantly elevated CO_2 compensation point, and highly reduced GDC activity in the isolated mitochondria (Eisenhut et al., 2013). Because *BOU* is co-expressed with genes encoding components of the GDC complex, and the *bou-2* mutant shows a similar metabolic phenotype as the *shm1* mutant, it was hypothesized that BOU transports a metabolite necessary for the proper functioning of GDC (Voll et al., 2006; Eisenhut et al., 2013). Recently, it was demonstrated that heterologously expressed BOU functions as a glutamate transporter (Porcelli et al., 2018). Glutamate is neither a substrate nor a product of the reaction catalyzed by GDC. Besides its role in amino acid and N metabolism, glutamate is necessary for the glutamylation of tetrahydrofolate (THF), a cofactor of GLDT and SHM (Suh

et al., 2001). Glutamylation of THF increases its stability. Moreover, THF-dependent enzymes generally prefer polyglutamylated folates over monoglutamylated folates as a substrate (Suh et al., 2001). However, because (1) BOU is not the only glutamate transporter in mitochondria, and (2) glutamylation of folates is not restricted to mitochondria, the exact physiological function of BOU remains unclear (Hanson and Gregory, 2011; Monné et al., 2018). Notably, a glutamate/glutamine shuttle across the mitochondrial membrane was previously suggested to support the reclamation of ammonia released during photorespiration (Linka and Weber, 2005).

Analysis of the biochemical and physiological functions of mitochondria frequently requires the isolation of intact mitochondria. Mitochondria can be isolated from leaf tissue in less than 1 h by differential centrifugation. This method yields mitochondria with good integrity and appropriate enzyme activity. However, mitochondria are frequently contaminated with plastids and peroxisomes. Hence, in many cases, a combination of differential centrifugation and Percoll density gradient is used (Millar et al., 2001; Werhahn et al., 2001; Keech et al., 2005). While this produces a pure fraction of respiratory active mitochondria with low plastid and peroxisome contamination, such procedures generally take several hours and require up to 50 g of starting material for producing sufficient yields (Keech et al., 2005). Moreover, traditional protocols are not practical for the isolation of mitochondria from mutants with severely impaired growth or from less abundant tissue types such as flowers and for the analysis of mitochondrial metabolites. Furthermore, media used for the isolation of mitochondria typically contain high concentrations of sugars and other metabolites that can potentially interfere with MS-based metabolite analyses.

Recently, Chen and coworkers reported a method for the rapid isolation of mitochondria from human HeLa cell cultures via co-immunopurification (co-IP) (Chen et al., 2016). The authors generated transgenic HeLa cell lines expressing a triple hemagglutinin (HA)-tagged enhanced green fluorescent protein (eGFP) fused to the outer mitochondrial membrane (OMM) localization sequence of OMP25 (3×HA-eGFP-OMP25). Because the epitope-tag was displayed on the surface of mitochondria, these transfected cell lines could be used to rapidly enrich mitochondria after cell homogenization. The HA-tagged mitochondria were captured and pulled down using magnetic beads coated with an anti-HA-tag antibody. Given the small size (1 µm diameter) and non-porous behavior of anti-HA-tag beads, these beads performed better than the porous agarose matrix for the enrichment of mitochondria. Thus, the authors established a method that ensures a high yield of pure mitochondria in approximately 12 min. The isolated mitochondria showed high purity, integrity, and functionality. Additionally, the authors developed a simple potassium-based buffer system

116 that maintains mitochondrial intactness and is compatible with downstream analyses, such
117 as metabolite analysis by LC/MS (Chen et al., 2016).

118 Building on this previous work, we developed an affinity-tagging strategy for the rapid
119 isolation of mitochondria from Arabidopsis. We generated transgenic Arabidopsis lines
120 carrying an HA-tagged translocase of the OMM 5 (TOM5) and isolated highly pure and intact
121 mitochondria from these lines in less than 25 min. The isolated mitochondria were
122 successfully subjected to proteomics and enzyme activity analyses. Moreover, we applied
123 the isolation strategy to the *bou-2* mutant, revealing differential protein abundance and
124 enzyme activities.

125

RESULTS

Identification of TOM5 a suitable anchor peptide and generation of affinity-tagged Arabidopsis lines

Recently, Chen and colleagues reported a rapid protocol for the isolation of intact mitochondria from transgenic HeLa cells expressing the mitochondrial fusion protein 3×HA-eGFP-OMP25 using co-IP. The Arabidopsis genome does not encode an ortholog of OMP25. Therefore, we screened the available Arabidopsis mitochondrial proteome data, including the OMM proteins with known topology and function, and identified TOM5 as a potential candidate for our mitochondria affinity-tagging approach. Together with TOM6, TOM7, TOM20, TOM22/9, and TOM40, TOM5 forms the protein import apparatus of plant mitochondria (Werhahn et al., 2003). In yeast (*Saccharomyces cerevisiae*), TOM5 is an integral protein of the OMM. It has a negatively-charged N-terminal domain, which faces toward the cytosol (Dietmeier et al., 1997) and can be fused to GFP without altering the subcellular localization of TOM5 (Horie et al., 2003). The protein import machinery is well conserved among eukaryotes. The predicted N-terminal cytosolic domain of Arabidopsis TOM5 is necessary for the recognition of cytosolically synthesized mitochondrial preproteins (Wiedemann et al., 2004). Therefore, we generated an N-terminal translational fusion of the Arabidopsis *TOM5* gene with triple HA-tagged *synthetic GFP* (*sGFP*) gene under the control of the Arabidopsis *UBIQUITIN10* promoter (*UB10p*) (*UB10p-3×HA-sGFP-TOM5*; Supplemental Fig. S1). The construct was used to stably transform Arabidopsis ecotype Columbia (Col-0) and *bou-2* mutant. Expression and localization of the fusion protein was verified in root and leaf tissues of 10-day-old Arabidopsis seedlings via confocal laser scanning microscopy. Transgenic Arabidopsis lines expressing the 3×HA-sGFP-TOM5 protein in leaf and root mitochondria of Col-0 and *bou-2* seedlings were identified based on the co-localization of the fluorescent signal of GFP signal with that of the mitochondrial marker CMXRos (Fig. 1A–D). CMXRos is a lipophilic cationic dye that accumulates in the mitochondria because of the negative membrane potential; thus, it solely stains mitochondria with an intact respiratory chain (Pendergrass et al., 2004). Because the fluorescent signals of the 3×HA-sGFP-TOM5 protein (green) fully overlapped with those of the MitoTracker (red), we conclude that overexpression of the *UB10p-3×HA-sGFP-TOM5* construct in Col-0 and *bou-2* does not affect mitochondrial intactness. In a few transgenic Col-0 lines, the fluorescent signal of sGFP formed a ring around the mitochondria, suggesting the localization of 3×HA-sGFP-TOM5 to the OMM (Fig. 1A, B). Notably, transgenic Col-0 or *bou-2* lines showed no apparent phenotypic differences compared with non-transgenic Col-0 or *bou-2* plants (control), respectively, under our culture conditions.

Figure 1

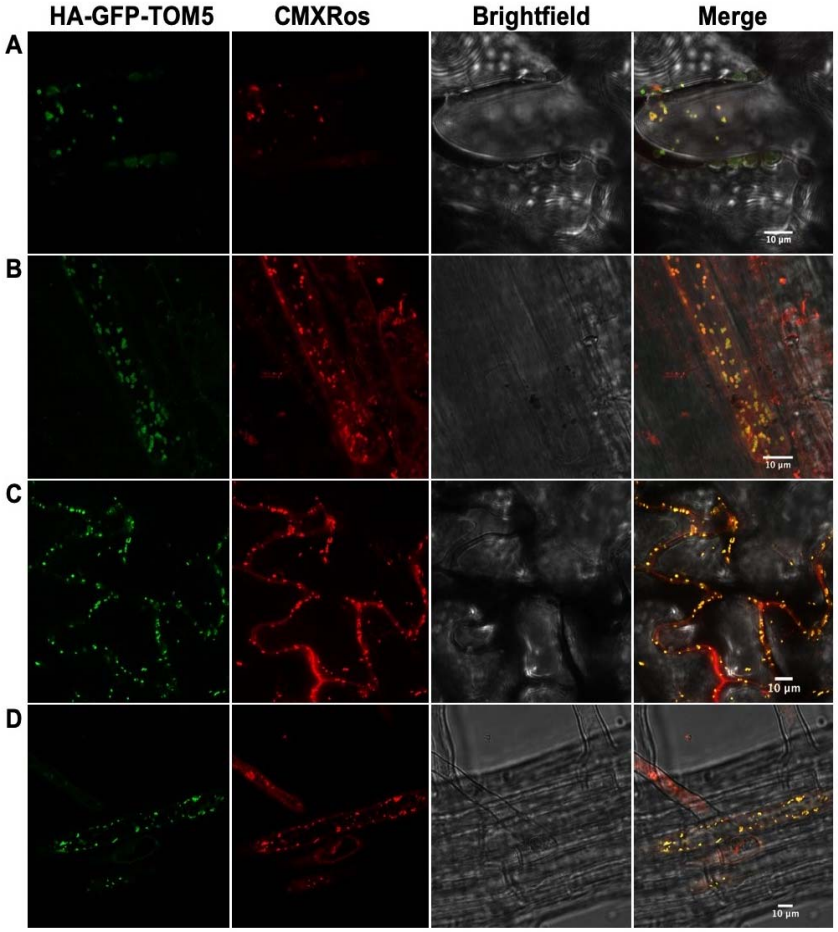

Figure 1: Confocal microscopy of epitope-tagged mitochondria in leaf and root tissues of transgenic Arabidopsis Col-0 and *bou-2* lines expressing the *UB10p-3×HA-sGFP-TOM5* construct. (A–D) Images of transgenic Col-0 leaf (A) and root (B) tissues and transgenic *bou-2* leaf (C) and root (D) tissues expressing the 3×HA-sGFP-TOM5 protein. Green color represents GFP signal, whereas red color represents the signal of mitochondrial marker MitoTracker™ Red CMXRos. Bright field and merged images are shown in yellow. Scale bar = 10 µm.

161 **Affinity-based purification of intact mitochondria**

Transgenic Col-0 and *bou-2* lines were used for the isolation of intact HA-tagged mitochondria via co-IP using magnetic anti-HA beads. We chose HA as the epitope-tag for purification because it has a high affinity for its cognate antibody, and Chen and coworkers previously demonstrated that the size and non-porous behavior of the anti-HA beads yields a high amount of mitochondria (Chen et al., 2016). Additionally, we used the LC/MS-compatible buffer containing KCl and KH_2PO_4 (KPBS) developed by Chen et al. (2016). Our purification procedure included five steps: homogenization of plant material in KPBS (1 min), filtration of the homogenate (1 min), two centrifugation steps (5 min and 9 min), and co-IP (7 min, including washing steps). Altogether, mitochondria were purified from plant material in less than 25 min (Fig. 2). If the first centrifugation step used to remove contaminating chloroplasts and cell debris is omitted, the isolation time can be reduced to 18 min. The purified mitochondria were verified by immunoblot analyses using known organelle-specific protein markers. Mitochondria were enriched via co-IP only from lines harboring the mitochondrial 3×HA-sGFP-TOM5 protein, as demonstrated by immunoblot analyses with antibodies directed against different mitochondrial marker proteins including isocitrate dehydrogenase (IDH; mitochondrial matrix), alternative oxidase 1/2 (AOX1/2; IMM), and voltage-dependent anion channel 1 (VDAC1; OMM). No enrichment of mitochondria was observed in control Col-0 lines, indicating that the beads bind specifically to the HA-tag on mitochondria in transgenic lines (Fig. 3). Comparison with classical mitochondria isolation protocols using differential centrifugation and density gradient purification revealed that the mitochondrial fraction enriched using our affinity-tagging method showed significantly less contamination with proteins from plastids, peroxisomes, endoplasmatic reticulum (ER), nuclei, and cytosol (Fig. 3). The following proteins were used as markers for different organelles: Rubisco large subunit (RbcL; plastid), catalase (Cat; peroxisome), lumenal-binding protein 2 (BiP2; ER), histone H3 (nucleus), and heat shock cognate protein 70 (HSC70; cytosol).

The intactness of mitochondria isolated from HA-tagged and control lines via co-IP was assessed based on the latency of malate dehydrogenase (MDH) activity. Additionally, isolation was performed in the presence of 1% (w/v) Triton X-114. MDH activity could be detected in mitochondria isolated from HA-tagged lines but not in those isolated from the control lines, thus verifying the results of our immunoblot analyses. When 1% (w/v) Triton X-114 was added to the washing buffer during co-IP, MDH activity was undetectable in both transgenic and control lines, as the detergent lyses the organelles (Fig. 4).

Typically, we used 5–10 g of Arabidopsis seedlings grown on agar plates for the isolation of mitochondria, and this yielded up to 700 µg of total mitochondrial protein. However,

Figure 2

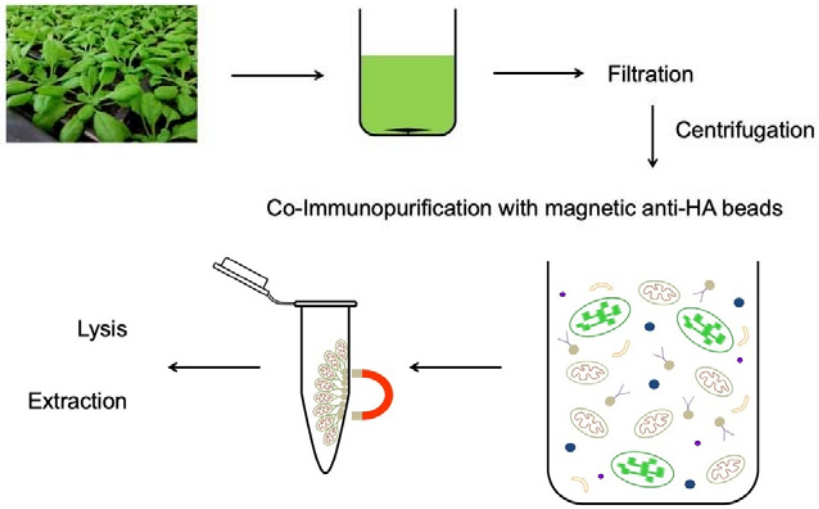

Figure 2: Workflow showing the rapid isolation of epitope-tagged mitochondria via co-Immunopurification (co-IP) from Arabidopsis. Transgenic lines harboring the *UB10p-3×HA-sGFP-TOM5* construct and non-transgenic (control) plants were harvested and homogenized in a Warren blender. The extract was filtered and centrifuged to obtain a crude mitochondrial fraction. Epitope-tagged mitochondria were purified via co-IP using magnetic anti-HA beads. The purified mitochondria were washed and either lysed for immunoblot analysis or extracted for proteomics.

197 mitochondria could also be isolated from 1 g of starting material, yielding up to 200 µg of
198 total mitochondrial protein. This is advantageous for very young seedlings or mutants with
199 severely impaired growth. Isolation from less than 1 g of starting material may also result in
200 an appropriate yield of mitochondria, but this was not tested in the current study.

201 Taken together, our data indicate that mitochondria can be rapidly isolated via co-IP using a
202 simple LC/MS-compatible buffer.

Figure 3

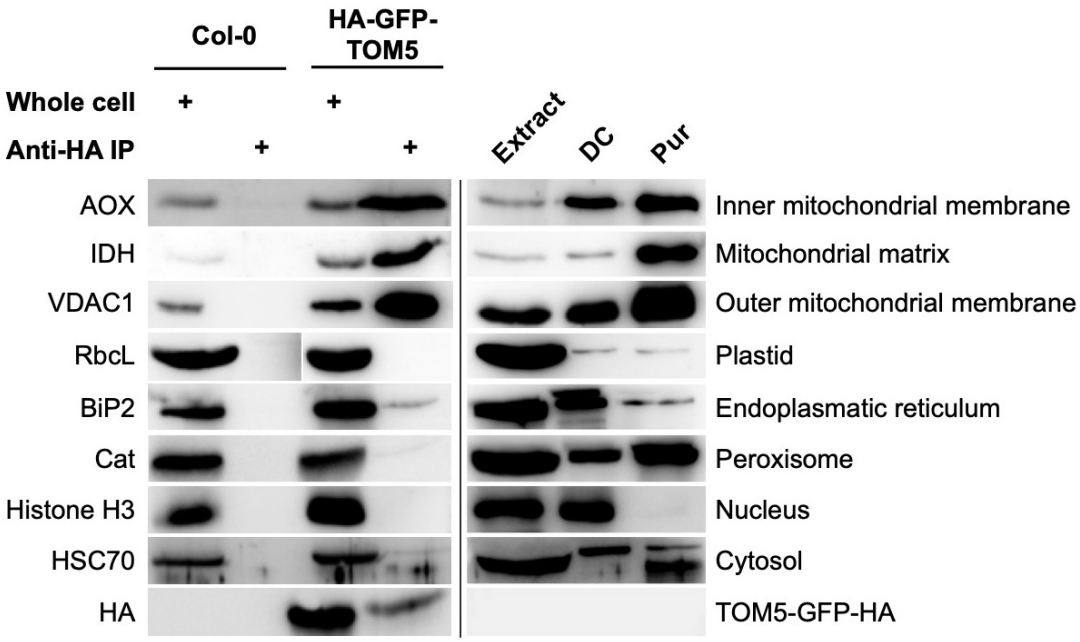

Figure 3: Immunoblot analysis of mitochondria isolated via co-IP or by differential centrifugation and gradient purification. Mitochondria were isolated from transgenic and non-transgenic (control) Col-0 and *bou-2* lines via co-IP using magnetic anti-HA beads (whole cell, Anti-HA IP) or using differential centrifugation and gradient purification (Extract, DC, Pur). Protein amounts were loaded as described in Material and Methods. Whole cell and extract samples were collected after tissue homogenization. Names of organelle marker proteins are shown on the left side of the blots, and their subcellular localization is indicated on the right.

Enzyme assays using mitochondria affinity-purified from transgenic Col-0 and *bou-2* mutant lines

We used our rapid mitochondria isolation method to study the effect of the mitochondrial carrier protein BOU on mitochondrial metabolism in Arabidopsis.

Figure 4

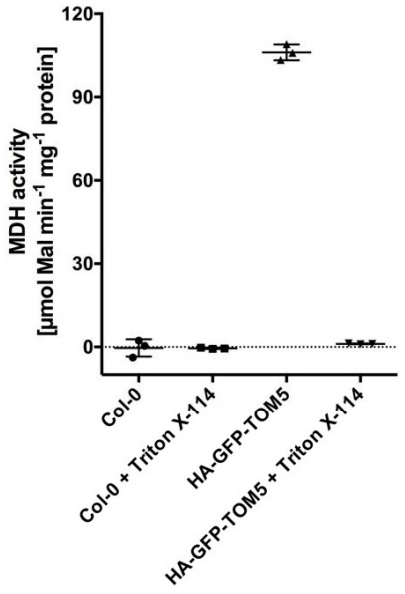

Figure 4: Latency of MDH activity in affinity-purified mitochondria. Mitochondria were rapidly isolated from transgenic and control Col-0 and *bou-2* plants via co-IP, with or without the addition of Triton X-114. The activity of MDH was calculated from the initial slope. Data represent mean ± SD of three replicates.

To assess the effect of the *bou-2* mutant allele on mitochondrial metabolism, we rapidly isolated mitochondria from 10-day-old transgenic Col-0 and *bou-2* seedlings grown under elevated CO_2 conditions (3,000 ppm) and those shifted to ambient CO_2 conditions (380 ppm CO_2 after 5 days). Mitochondria were lysed and used to measure the activity of MDH, aspartate aminotransferase (AspAT), glutamate dehydrogenase (GluDH), alanine aminotransferase (AlaAT), γ-aminobutyric acid transaminase (GABA-T), and formate dehydrogenase (FDH). Enzyme activities were calculated from the initial slopes. Enzyme activities in transgenic *bou-2* mutant lines were compared with those in transgenic Col-0 lines, which were set to 100%.

The activities of MDH and FDH were not affected in transgenic *bou-2* mutant lines under any of the conditions tested (Fig. 5A, B). The activities of AspAT and GABA-T in transgenic

Figure 5

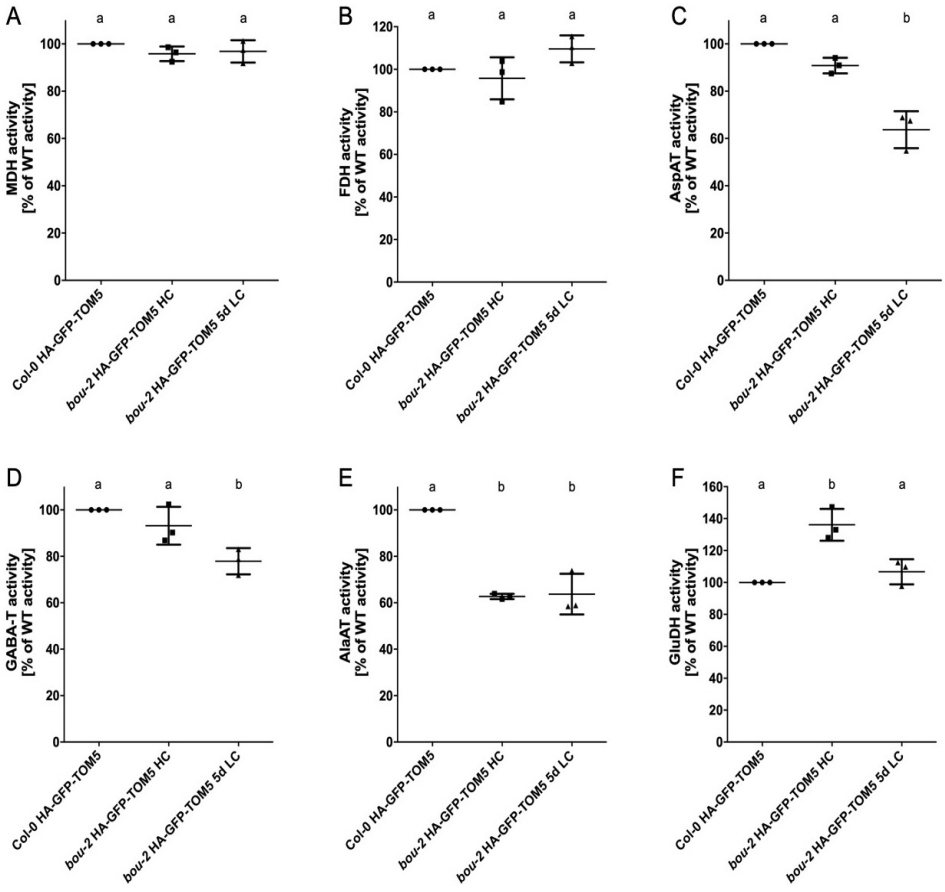

Figure 5: Characterization of enzyme activities in mitochondria isolated from 10-day-old transgenic Col-0 and *bou-2* lines grown at 3,000 ppm (HC) and after shift to 380 ppm (5d LC) via co-IP. (A) Malate dehydrogenase (MDH) activity. (B) Formate dehydrogenase (FDH) activity. (C) Aspartate aminotransferase (AspAT) activity. (D) γ-aminobutyric acid transaminase (GABA-T) activity. (E) Alanine aminotransferase (AlaAT) activity. (F) Glutamate dehydrogenase (GluDH) activity. Activities were calculated from initial slopes. Enzyme activities in transgenic Col-0 were set to 100%. Data represent mean ± SD of three biological replicates. Different letters indicate statistically significant differences between means for each enzyme ($P < 0.05$; one-way ANOVA).

218 mutant lines were similar to those in transgenic Col-0 lines, when mitochondria were isolated

from seedlings grown under elevated CO_2 conditions, but were significantly reduced in transgenic mutant lines after the shift to ambient CO_2 conditions (Fig. 5C, D). The activity of AlaAT was significantly reduced (Fig. 5E), whereas that of GluDH was significantly increased in transgenic mutant lines under elevated CO_2 conditions; however, both enzyme activities reverted back to the levels in transgenic Col-0 when seedlings were shifted to ambient CO_2 conditions (Fig. 5F). Together, our results suggest a possible involvement of BOU in mitochondrial amino acid and N metabolism.

In addition, we found that the activity of MDH was strongly reduced in 4-week-old transgenic *bou-2* mutant plants grown under elevated CO_2 conditions (Supplemental Fig. S2). However, no change was observed in MDH activity in 10-day-old transgenic *bou-2* plants, suggesting pleiotropic effects in older leaf tissues due to accumulating photorespiratory intermediates.

Proteomic analysis of mitochondria affinity-purified from transgenic Col-0 and *bou-2* mutant lines

Mitochondria were isolated from 10-day-old transgenic Col-0 and *bou-2* seedlings grown under elevated CO_2 conditions in four independent biological replicates. Proteome analysis of the isolated mitochondria revealed 15,688 peptides belonging to 1,240 proteins present in at least three of the four replicates (Supplemental Table S1, Supplemental Table S2).

Subcellular localization of the quantified proteins was annotated using the SUBAcon database (Hooper et al., 2017). Summing up the label-free quantitation (LFQ) intensities of the spectra showed that 80% of all quantified peptides resulted from proteins localized or predicted to be localized to the mitochondria, 11.5% from plastid-localized proteins, and 5.7% from proteins with no clear subcellular localization (designated as ambiguous). Additionally, more than 90% of the quantified peptides were assigned to the mitochondria. Contamination of the mitochondrial proteins by proteins from peroxisomes, ER, Golgi, vacuoles, endomembranes, plasma membranes, nuclei, and cytosol was less than 1% each (Supplemental Table S1, Supplemental Table S2). These results indicate high purity of the rapidly isolated mitochondria, which was comparable with the purity of classically isolated mitochondria (Klodmann et al., 2011; Senkler et al., 2017).

Next, we compared our proteome data with previous proteomic analyses and quantified proteins and some of the subunits of known mitochondrial complexes (Supplemental Table S1, Supplemental Table S2). The OXPHOS pathway of mitochondria consists of five protein complexes (I–V) located in the IMM. Complexes I to IV represent oxidoreductases, which comprise the respiratory chain that regenerates oxidized forms of cofactors involved in mitochondrial metabolism, thereby creating an electron flow. This leads to the simultaneous

253 export of protons into the intermembrane space (IMS). The built-up proton gradient is used
254 by Complex V to generate ATP. Complex I is the largest complex involved in the OXPHOS
255 pathway and comprises at least 47 protein subunits that form the so-called membrane and
256 peripheral arms (Peters et al., 2013; Meyer et al., 2019). Except NDUA1, NDUB2, Nad4L,
257 and Nad6 (At3g08610, At1g76200, AtMg00650, and AtMg00270, respectively), we could
258 identify all Complex I subunits in our proteomic data set. Additionally, we identified eight
259 previously proposed assembly factors (Meyer et al., 2019), five γ-carbonic anhydrases, and
260 five additional proteins proposed to form a matrix-exposed domain attached to Complex I
261 (Sunderhaus et al., 2006). Complex II is composed of eight subunits (Millar et al., 2004). In
262 addition to its function in the OXPHOS pathway, Complex II also participates in the
263 tricarboxylic acid cycle (TCA). Six out of eight subunits of Complex II and the assembly
264 factor SDHAF2 were identified in our data set. Additionally, peptides of all proteins and
265 isoforms of Complex III, eight of its assembly factors, and proteins previously defined as
266 alternative pathways (Meyer et al., 2019) were identified in our data set. Complex V consists
267 of 15 subunits, of which 13 were identified in our proteomic data set; Atp6 (AtMg00410 and
268 AtMg011701) and Atp9 (AtMg01080) were the only two subunits that could not be identified.
269 In addition, we found three of the five proposed assembly factors (Meyer et al., 2019). The
270 cytochrome c oxidase complex (Complex IV) consists of 16 proposed subunits in
271 Arabidopsis (Mansilla et al., 2018). Of these, 9 subunits and 11 assembly factors of Complex
272 IV were identified in our proteomic data set. Furthermore, we identified three proteins
273 involved in the assembly of OXPHOS supercomplexes (Meyer et al., 2019).

274 Except the abovementioned subunits of the SDH complex, all proteins of the TCA cycle and
275 GDC multienzyme system were identified in the rapidly isolated mitochondria. Additionally,
276 our proteomic data set contained a number of pentatricopeptide and tetratricopeptide repeat
277 proteins involved in RNA metabolism as well as heat shock proteins and ribosomes involved
278 in protein control and turnover (Supplemental Table S1, Supplemental Table S2).

279 In Arabidopsis, the majority of mitochondrial proteins are encoded by nuclear genes,
280 translated in the cytosol, and then imported into the mitochondria. The import and sorting of
281 nuclear-encoded mitochondrial preproteins requires functional TOM and sorting and
282 assembly machinery (SAM) in the OMM, mitochondrial IMS import and assembly (MIA)
283 machinery in the IMS, and translocase of the IMM (TIM) in the IMM (Murcha et al., 2014). All
284 mitochondrial preproteins enter the mitochondria via the TOM complex in the OMM. In the
285 IMS, membrane proteins are sorted via the small TIM proteins toward the SAM or TIM22
286 complex for incorporation into the OMM or IMM. Soluble proteins of the mitochondrial matrix
287 are imported via the TIM17:23 complex, and proteins that remain in the IMS are processed
288 via the MIA machinery (Murcha et al., 2014). In this study, we identified all of these proteins

in our proteome data set, except the OMM protein TOM6, IMS protein ERV1, IMM protein PRAT5, and matrix proteins MGE1 and ZIM17. Additionally, we identified plant-specific import components, including OM64, PRAT3, and PRAT4, in the OMM (Murcha et al., 2015) and proteins of the mitochondrial contact site and cristae organizing system (MICOS), which connects the IMM to OMM (van der Laan et al., 2016). Other notable OMM proteins identified in our proteomic data set included GTPases MIRO1 and MIRO2, lipid biosynthesis protein PECT, and β-barrel proteins VDAC1–4 (Supplemental Table S1, Supplemental Table S2). Recently, it was shown that the cytosolic protein GAPC interacts with VDAC (Schneider et al., 2018); we also identified GAPC in our proteomic data set.

Overall, we conclude that mitochondria isolated using our rapid isolation method are suitable for proteomic analyses.

Differential analysis of the mitochondrial proteome of transgenic Col-0 and *bou-2* lines

To assess the effect of *bou-2* mutation on the mitochondrial proteome, we performed comparative proteomic analysis of transgenic Col-0 and *bou-2* lines. A total of 47 proteins showed significantly increased abundance in the mutant, of which five were localized to the mitochondria. Additionally, 44 proteins showed significantly decreased abundance in the transgenic *bou-2* samples, of which 22 were predicted to be localized to the mitochondria (Table 1); among these proteins, BOU was the least abundant. The *bou-2* line is a GABI-Kat line that carries a T-DNA insertion in the second exon of the *BOU* gene (Kleinboelting et al., 2012; Eisenhut et al., 2013). We identified two peptides of BOU in at least three of the four replicates of transgenic *bou-2* samples. Both peptides were translated from the first exon of the gene. Because the T-DNA was inserted in the second exon of the gene, it is possible that the first exon was translated. However, a functional protein is not synthesized in the knockout mutant (Eisenhut et al., 2013). Among the mitochondrial proteins showing significantly reduced abundance in transgenic *bou-2* seedlings, we identified six proteins of the OXPHOS pathway (three Complex I proteins and one protein each of Complex II, III, and V), two proteins involved in protein translocation, two proteins involved in metabolite transport, two proteins involved in lipid metabolism, three proteins involved in protein turnover/synthesis, one protein involved in the TCA cycle, and six proteins (including FDH) involved in other processes. Among the proteins with significantly increased abundance in transgenic *bou-2* mutant, we identified two proteins involved in RNA/DNA metabolism, one protein involved in THF metabolism, one MIRO-related GTPase, and one LETM1-like protein (Table 1).

Previously, Eisenhut and colleagues showed that GDC activity is reduced in mitochondria isolated from 4-week-old *bou-2* mutant plants (Eisenhut et al., 2013). The authors showed that the *bou-2* mutant accumulated higher amounts of glycine than the wild type and exhibited differential amount and status of the P-protein. Immunoblot analysis showed no differences in the levels of other GDC proteins in the *bou-2* mutant compared with the wild type (Eisenhut et al., 2013). In our proteomic data set, none of the proteins of the GDC complex or SHMT showed significant differences between transgenic Col-0 and *bou-2* seedlings (Table 2). However, the amounts of GLDP1, GLDP2, GDCH1, GDCL1, GDCL2, and GLDT were slightly reduced, whereas those of SHM1, SHM2, and GDCH3 were increased in the mutant compared with Col-0. Among these proteins, the strongest reduction was detected in the amount of GDCH1. However, differences in protein levels between transgenic Col-0 and *bou-2* seedlings were not statistically significant. Only one peptide related to GDCH2 was detected in our data set; however, because it was detected in only one of the four replicates, it is not listed Supplemental Table S1.

In this study, we showed that mitochondria of the *bou-2* mutant displayed reduced AlaAT activity, increased GluDH activity, and no change in MDH, AspAT, GABA-T, and FDH activities under elevated CO_2 conditions compared with that under ambient CO_2 conditions (Fig. 4A–F). Except FDH, none of the assayed enzymes showed significantly altered amounts in our proteomic data set (Table 2). The amount of FDH was significantly reduced in transgenic *bou-2* samples; however, its activity was not altered in the mutant under both elevated and ambient CO_2 conditions, indicating post-translational modification of FDH. The level of AlaAT was slightly increased in the mutant but showed only 60% activity compared with Col-0 under both elevated and ambient CO_2 conditions. The activities of MDH, AspAT, and GABA-T did not differ between transgenic Col-0 and *bou-2* mutant under elevated CO_2 conditions, although these proteins were more abundant in transgenic mutant samples. The activity of GluDH was significantly increased in the mutant compared with Col-0 under elevated CO_2 conditions, which may be associated with the increased amount of protein detected in the transgenic *bou-2* seedlings in our proteomic data set. However, this increase was not statistically significant.

Overall, we conclude that differences in the activities of MDH, AspAT, GluDH, AlaAT, GABA-T, and AlaAT measured in this study and that of GDC measured in a previous study most likely do not relate to changes in protein abundance in mitochondria of Col-0 vs. *bou-2* mutant but instead might be caused by metabolic impairment or post-translational modifications.

DISCUSSION

Recently, analyses of mitochondrial proteome content, complexome composition, post-translational modifications, energy metabolism, OXPHOS complex formation and function, protein translocation, and metabolite shuttles have been conducted to further our understanding of mitochondrial metabolism in Arabidopsis (König et al., 2014; Fromm et al., 2016; De Col et al., 2017; Rao et al., 2017; Senkler et al., 2017; Porcelli et al., 2018; Hu et al., 2019; Kolli et al., 2019; Meyer et al., 2019; Nickel et al., 2019). Many of these analyses required the isolation of intact mitochondria. Here, we report a procedure for the rapid isolation of HA-tagged mitochondria from transgenic Arabidopsis lines via co-IP. Mitochondria isolated using this method showed high enrichment of mitochondrial marker proteins, with only minor contamination, as demonstrated by immunoblot and quantitative proteomic analyses (Fig. 3, Supplemental Table S1, Supplemental Table S2).

The method reported here enables the isolation of intact mitochondria from Arabidopsis seedlings in less than 25 min (Fig. 2, Fig. 3). Moreover, by omitting the first centrifugation step, the isolation time could be shortened to 18 min, although the resulting mitochondrial fraction contained a higher level of other contaminating cellular components. The mitochondrial fraction used for proteomic analyses in this study was obtained using the slightly longer protocol that results in lower contamination with non-mitochondrial proteins. Nevertheless, this isolation method is significantly faster than the standard isolation procedures that generally take up to several hours. To date, we have been able to successfully isolate mitochondria from whole seedlings, leaves, and roots (data not shown). Moreover, this method could be used for the rapid isolation of mitochondria from other plant tissues such as flowers and developing seeds because (1) the expression of the affinity tag is driven by the ubiquitous *UB10p* promoter (Supplemental Fig. S1) and (2) only a small amount of starting material (as low as 1 g) is needed. Additionally, this method is advantageous for the isolation of mitochondria from very young tissues or mutants with growth defects or reduced biomass accumulation. The rapid isolation method is superior to the standard isolation protocols with respect to the yield of mitochondria; we were able to isolate 200 µg of total mitochondrial protein from 1 g of starting material and up to 700 µg total mitochondrial protein from 10 g of whole Arabidopsis seedlings. By contrast, the standard isolation protocols yield only 1.2 mg mitochondria from 50 g of leaves (Keech et al., 2005). Generally, a higher yield is expected using our isolation method, as the HA-tag has high affinity for its cognate antibody. Further optimization of the protocol and bead to extract ratio may result in even higher yields.

The purity of affinity-purified mitochondria was similar to that of mitochondria isolated using standard protocols including density gradients (Senkler et al., 2017). Immunoblot analysis revealed only minor contamination with proteins of the ER or peroxisomes in affinity-purified mitochondria (Fig. 3). These results were corroborated by quantitative proteomic analysis. Less than 3% of all quantified proteins were assigned to peroxisomes, ER, Golgi, vacuoles, endomembranes, plasma membranes, nuclei, and cytosol. The highest contamination was due to plastid-localized proteins (Supplemental Table S1, Supplemental Table S2). However, we cannot exclude the possibility that some of the contaminants bound non-specifically to the beads, despite extensive washing. Approximately 80% of the identified proteins and 90% of the identified peptides showed mitochondrial localization (Supplemental Table S1, Supplemental Table S2). Thus, we conclude that the purity of mitochondria isolated using the rapid affinity purification method is comparable with that of mitochondria isolated using traditional methods. We cannot comment on the physiological activity and coupling state of affinity-purified mitochondria because we could not efficiently elute the mitochondria from the magnetic beads with HA peptide. However, mitochondria could be efficiently eluted using SDS-PAGE or detergent lysis buffer. Elution of intact mitochondria might be achievable by integrating a protease cleavage site between the HA-tag and GFP; this will be explored in future studies.

In our data set, we were able to identify 96% and 99% of the proteins detected by Klodmann et al. (2011) and Senkler et al. (2017), respectively, in previous analyses of mitochondrial proteomes and their complexome composition (Supplemental Table S1, Supplemental Table S2). On the basis of a recent review on the composition and function of OXPHOS in mitochondria (Meyer et al., 2019), we were able to identify 86% of all the predicted subunits and assembly factors. To date, all of the proteins reviewed in Meyer et al. (2019) have not been confirmed, and it might require an in-depth analysis or membrane enrichment to confirm their presence in mitochondria in proteomic studies. Previously, it was reported that the subunit ND4L is difficult to detect in proteomic studies because of its hydrophobic nature (Peters et al., 2013). Consistent with this observation, we also could not identify this protein in our proteome or in the list of quantified peptides (Supplemental Table S1, Supplemental Table S2). However, we were able to detect all proteins of the TCA cycle (except two subunits of Complex II), all GDC proteins, majority of the proteins and subunits of the TIM/TOM protein import apparatus, metabolite transporters of amino acids, dicarboxylic acids, cofactors, ions and energy equivalents (e.g., BOU, BAC, UCP, DCT, SAMC, NDT, APC, AAC, and PHT), as well as many proteins involved in protein synthesis/turnover and DNA/RNA metabolism (Supplemental Table S1, Supplemental Table S2). Thus, our rapidly isolated mitochondria showed good purity, integrity, and functionality.

Among all of the identified proteins, 20% could not be assigned to mitochondria. These proteins included components of PSI and PSII; these could be clearly categorized as contamination. However, we also identified proteins with unknown function and no clear prediction of localization. In addition, we detected proteins such as GAPC, which was previously shown to interact with the OMM protein VDAC (Schneider et al., 2018). Therefore, we predict that some of the proteins classified as contaminants might represent novel mitochondrial proteins, for example, as part of OMM protein complexes in the cytosol or as components of complexes at organellar contact sites. However, this needs to be evaluated in more detail in the future.

Application of the novel method to a mutant lacking the mitochondrial glutamate transporter BOU resulted in the detection of surprisingly few changes in protein abundances compared with Col-0. Only 22 mitochondrial proteins showed a significant reduction in abundance in the *bou-2* mutant, whereas five proteins were significantly increased in abundance. However, only changes in a mitochondrial folylpolyglutamate synthetase (FGPS) and in FDH, which contributes to the production of CO_2 by oxidizing formate, might be connected to photorespiration. Formate is released from 10-formyl-THF by 10-formyl deformylase, an enzyme involved in the maintenance of the THF pool in mitochondrial matrix (Collakova et al., 2008). Reduced GDC activity in *bou-2* might result in a lower production of formate and finally a reduced abundance of FDH. FGPS is involved in vitamin B9 metabolism by catalyzing the glutamylation of THF, a cofactor of GLDT and SHM (Hanson and Gregory, 2011). No significant changes were detected in the abundance of any of the proteins of the GDC multienzyme system. SHM1, SHM2, and GDCH3 were slightly more abundant in the mutant than Col-0, whereas the others seem to be slightly reduced; however, this trend did not meet the significance threshold (Table 2). The observed changes were not pronounced and did not explain why the GDC activity was reduced to approximately 15% of the Col-0 level in the *bou-2* mutant. A possible explanation could be that Eisenhut and coworkers used 4-week-old rosettes (Eisenhut et al., 2013), whereas we used 10-day-old seedlings in the current study. This possibility is supported by the observation that no difference in MDH activity could be detected between 10-day-old mutant and Col-0 seedlings (Fig. 5A). However, in 4-week-old leaves, the MDH activity was significantly reduced in the mutant compared with Col-0 (Supplemental Fig. S2). In contrast to GDC, the abundance of FDH was significantly reduced in the mutant, whereas its activity was unaltered compared with Col-0 (Table 1, Fig. 5B). Previously, FDH was identified in a lysine acetylome study of Arabidopsis mitochondria from 10-day-old Col-0 seedlings (König et al., 2014). This might indicate that FDH activity is more likely regulated by post-translational modifications than by protein abundance.

The BOU protein was recently assigned the function of a glutamate transporter (Porcelli et al., 2018). Glutamate is indirectly linked to photorespiration, as it is needed for the polyglutamylation of THF, which increases its stability and promotes the activity of THF-dependent enzymes (Hanson and Gregory, 2011). However, in addition to BOU, mitochondria-localized uncoupling proteins 1 and 2 show glutamate uptake activity in Arabidopsis (Monné et al., 2018). This raises the question why knockout of the *BOU* gene leads to a photorespiratory phenotype in young tissues, if BOU is not the only glutamate transporter of mitochondria. Additionally, polyglutamylation is not restricted to mitochondria, as Arabidopsis contains three isoforms of FGPS localized to the mitochondria, plastids, and cytosol (Hanson and Gregory, 2011). Folate transporters prefer monoglutamylated forms of THF, whereas enzymes generally prefer polyglutamylated forms (Suh et al., 2001). These data indicate that BOU performs other functions, in addition to glutamate transport *in vivo*. We exclude its function as a mitochondrial glutamate/glutamine shuttle, as BOU shows no glutamine uptake activity (Porcelli et al., 2018). However, it is possible that BOU is involved in folate metabolism, as folate biosynthesis occurs only in mitochondria (Hanson and Gregory, 2011). This possibility, however, needs to be investigated in future studies.

CONCLUSIONS

Our experiments show that affinity-tagging is a powerful tool not only for the analysis of protein-protein interactions but also for the isolation of functional organelles from Arabidopsis. The mitochondria isolated using this method showed high purity and integrity. Future studies will be required to assess the physiological state of the isolated mitochondria after elution from magnetic beads and to determine the applicability of this method for metabolite analyses. To conduct metabolite analyses, it is encouraging that the LC/MS-compatible buffer system developed previously for mammalian mitochondria (Chen et al., 2016) can also be used for the isolation of mitochondria from plant tissues. Expressing the affinity tag under the control of cell-specific promoters will allow the isolation of mitochondria from specific cell types, such as meristems or guard cells (Yang et al., 2008; Schürholz et al., 2018). The use of cell-specific promoters in our construct will help unravel the complex role of mitochondria in various cell types. We expect that similar tagging strategies will be applicable to other plant cell organelles, such as plastids and peroxisomes. Moreover, simultaneous expression of several different affinity tags will facilitate the affinity purification of different organelles from a single extract.

MATERIAL AND METHODS

Pant growth conditions

Arabidopsis ecotype Col-0 and *bou-2* mutant (GABI-Kat line number 079D12; http://www.gabi-kat.de/db/lineid.php) (Kleinboelting et al., 2012) were used in this study. Seeds were sterilized by washing with 70% (v/v) ethanol supplemented with 1% (v/v) Triton X-100 twice for 10 min each, followed by washing with 100% ethanol twice for 10 min each. Seeds were grown on half-strength Murashige and Skoog (1/2 MS) medium (pH 5.8) supplemented with 0.8% (w/v) agar. Seeds were subjected to cold stratification for 2 days at 4°C. After germination, seedlings were grown under 12 h light/12 h dark photoperiod under 100 µmol m^{-2} s^{-1} light intensity and 3,000 ppm CO_2-enriched atmosphere, unless otherwise stated.

Construction of transgenic lines

The HA epitope-tag was amplified with a start codon from the Gateway binary vector pGWB15. The coding sequence (CDS) of sGFP, minus the start and stop codons but including a linker peptide (GGSG) at the 5' and 3' ends, was amplified from the Gateway binary vector pGWB4. The CDS of *TOM5* (minus the start codon) was amplified from Arabidopsis cDNA. Starting from the 5'-end to the 3'-end, the amplified 3×HA-tag, sGFP, and TOM5 were cloned into the pUTKan vector under the control of the Arabidopsis *UB10p* using restriction endonucleases. The construct was introduced into *Agrobacterium tumefaciens*, strain GV3101::pMP90, which was then introduced into Col-0 and *bou-2* plants via *Agrobacterium*-mediated transformation using the floral dip method, as described previously (Clough and Bent, 1998).

Confocal laser scanning microscopy

The expression of 3×HA-sGFP-TOM5 was verified via confocal laser scanning microscopy using the Zeiss LSM 78 Confocal Microscope and Zeiss ZEN software. The Col-0 and *bou-2* seedlings regenerated from independent transformation events were incubated with 200 nM MitoTracker Red CMXRos (Molecular Probes) in 1/2 MS supplemented with 3% (w/v) sucrose for 15 min. Images were captured using the following excitation/emission wavelengths: sGFP (488 nm/490–550 nm) and MitoTracker Red CMXRos (561 nm/580–625 nm). Pictures were processed using the ImageJ software (https://imagej.nih.gov/ij/).

Rapid isolation of mitochondria using co-IP

Epitope-tagged mitochondria were rapidly isolated using co-IP, as described previously (Chen et al., 2016). Briefly, 1–10 g of Arabidopsis seedlings were harvested and

homogenized in KPBS (10 mM KH_2PO_4 [pH 7.25] and 136 mM KCl) using a Warren blender. The resulting homogenate was filtered through three layers of miracloth supported by a nylon mesh and centrifuged at 2,500 × *g* for 5 min. The pellet containing cell debris and chloroplasts was discarded. The supernatant was subsequently centrifuged at 20,000 × *g* for 9 min. The pellet representing the crude mitochondrial fraction was resuspended in KPBS using a fine paintbrush and homogenized using a Potter-Elvehjem. Crude mitochondria were incubated with pre-washed magnetic anti-HA beads (ThermoFisher Scientific) on an end-over-end rotator for 5 min. Magnetic beads were separated using a magnetic stand and washed at least three times with KPBS. In the detergent treatment control, KPBS was supplemented with 1% (v/v) Triton X-114 in all washing steps. The purified mitochondria were lysed using mitochondria lysis buffer (50 mM TES/KOH [pH 7.5], 2 mM EDTA, 5 mM $MgCl_2$, 10% [v/v] glycerol, and 0.1% [v/v] Triton X-100) for enzyme activity assays and immunoblot analysis or directly frozen in liquid nitrogen for proteome and metabolite analyses. All steps were carried out at 4°C. The amount of protein recovered after lysis was determined using the Quick Start™ Bradford Protein Assay Kit (Bio-Rad), with bovine serum albumin (BSA) as the standard.

Isolation of mitochondria using the traditional approach

Mitochondria were isolated from 10-day-old Col-0 seedlings via differential centrifugation and Percoll gradient purification, as described previously (Kühn et al., 2015).

Immunoblot analysis

25 µg of total leaf extract and 6.45 µg of isolated mitochondria fractions were heated at 96°C in SDS-PAGE loading buffer for 10 min and separated on 12% SDS-polyacrylamide gels (Laemmli, 1970). Proteins were transferred to 0.2 µm polyvinylidene difluoride membranes (PVDF) or 0.45 µm nitrocellulose membranes using standard protocols. Protein transfer was verified by staining the membranes with Ponceau S red. Membranes were blocked according to the manufacturer's instructions for 1 h, washed with Tris-buffered saline containing 0.1% (v/v) Tween-20 (TBST) and subsequently incubated with either a primary antibody or a single-step antibody overnight at 4°C. Antibodies against marker proteins were diluted as follows: anti-AOX (1:1,000), anti-IDH (1:5,000), anti-VDAC1 (1:5,000), anti-HA-HRP (1:5,000), anti-RbcL (1:7,500), anti-Cat (1:1,000), anti-BiP2 (1:2,000), anti-Histone H3 (1:5,000), and anti-HSC70 (1:3,000). Membranes were washed with TBST twice for 10 min each and incubated with the secondary goat anti-Rabbit-HRP antibody (1:5,000) at room temperature for 1 h or at 4°C overnight. Subsequently, membranes were washed with TBST five times for 5 min each and visualized using a chemiluminescence detection system

(Immobilon Western HRP Substrate, Merck Millipore). All steps were carried out with phosphate-buffered saline (PBS), when using anti-Cat antibody.

Enzyme assays

Activities of mitochondrial enzymes were measured using a spectrophotometer, based on the absorbance at 340 nm. The activity of MDH was measured based on the oxidation of NADH to NAD^+ at 340 nm, as described previously (Tomaz et al., 2010). The reaction mixture contained 50 mM KH_2PO_4 (pH 7.5), 0.2 mM NADH, 5 mM EDTA, 10 mM $MgCl_2$, 2 mM OAA (Tomaz et al., 2010), and 0.1–0.4 µg total mitochondrial protein. AspAT activity was measured in a reaction coupled with MDH, as described previously (Wilkie and Warren, 1998), with 0.3–1 µg total mitochondrial protein per assay. No external pyridoxal-5'-phosphate was added to the reaction mixture. GluDH activity was measured as described previously (Turano et al., 1996), based on the reduction of NAD^+ to NADH at 340 nm. To determine the amination activity, 0.5–2 µg total mitochondrial protein was used per assay. GABA-T activity was measured in a reaction coupled with succinate-semialdehyde dehydrogenase (SSADH), as described previously (Clark et al., 2009). The assay buffer contained 50 mM TAPS (pH 9), 0.2 mM NAD^+, 0.625 mM EDTA, 8 mM GABA, 2 mM pyruvate, 1 U/ml SSADH, and 2–5 µg total mitochondrial protein. The NAD^+-dependent SSADH was purified from *Escherichia coli*, as described previously (Clark et al., 2009). The recombinant purified protein catalyzed the production of NADH with a specific activity of 1.6 U/mg protein. AlaAT activity was measured in reaction coupled with lactate dehydrogenase, as described previously (Miyashita et al., 2007), with 1–5 µg total mitochondrial protein. FDH activity was measured based on the reduction of NAD^+ to NADH at 340 nm and 30°C, with 1–5 µg total mitochondrial protein. The assay buffer contained 100 mM KH_2PO_4 (pH 7.5), 1mM NAD^+, and 50 mM sodium formate.

Sample preparation for LC/MS analysis

To elute proteins from magnetic beads, 30 µl of Laemmli buffer was added to the reaction mixture, and samples were incubated at 95°C for 10 min. Subsequently, 20 µl of protein sample was loaded on an SDS-polyacrylamide gel for in-gel digestion. The isolated gel pieces were reduced using 50 µl of 10 mM DTT, then alkylated using 50 µl of 50 mM iodoacetamide, and finally digested using 6 µl of trypsin (200 ng) in 100 mM ammonium bicarbonate. The peptides were resolved in 15 µl of 0.1% trifluoracetic acid and subjected to LC/MS analysis.

595 **LC/MS analysis**

596 The LC/MS analysis was performed on a Q Exactive Plus mass spectrometer (Thermo
597 Scientific, Bremen, Germany) connected to an Ultimate 3000 Rapid Separation LC system
598 (Dionex; Thermo Scientific, Idstein, Germany) and equipped with an Acclaim PepMap 100
599 C18 column (75 µm inner diameter × 25 cm length × 2 mm particle size; Thermo Scientific,
600 Bremen, Germany). The length of the isocratic LC gradient was 120 min. The mass
601 spectrometer was operated in positive mode and coupled with a nano electrospray ionization
602 source. Capillary temperature was set at 250°C, and source voltage was set at 1.4 kV. The
603 survey scans were conducted at a mass to charge (m/z) ranging from 200 to 2000 and a
604 resolution of 70,000. The automatic gain control was set at 3,000,000, and the maximum fill
605 time was set at 50 ms. The ten most intensive peptide ions were isolated and fragmented by
606 high-energy collision dissociation (HCD).

607 **Computational MS data analysis**

608 Peptide and protein identification and quantification was performed using MaxQuant version
609 1.5.5.1 (MPI for Biochemistry, Planegg, Germany) with default parameters. The identified
610 Arabidopsis peptides and proteins were queried against a specific proteome database
611 (UP0000006548, downloaded 12/11/17) from UniProt. The oxidation and acetylation of
612 methionine residues at the N-termini of proteins were set as variable modifications, while
613 carbamidomethylations at cysteine residues were considered as fixed modification. Peptides
614 and proteins were accepted with a false discovery rate of 1%. Unique and razor peptides
615 were used for label-free quantification, and peptides with variable modifications were
616 included in the quantification. The minimal ratio count was set to two, and the 'matched
617 between runs' option was enabled.

618 Normalized intensities, as provided by MaxQuant, were analyzed using the Perseus
619 framework (version 1.5.0.15; MPI for Biochemistry, Planegg, Germany). Only proteins
620 containing at least two unique peptides and a minimum of three valid values in at least one
621 group were quantified. Proteins which were identified only by site or marked as a
622 contaminant (from the MaxQuant contaminant list) were excluded from the analysis.
623 Differential enrichment of proteins in the two groups (*Col-0*; *bou-2*) was assessed using
624 Student's *t*-test. Significance analysis was applied on $\log_2$-transformed values using an S0
625 constant of 0 and a false discovery rate of 5%, as threshold cutoffs.

626 The MS proteomics data has been deposited to the ProteomeXchange Consortium via the
627 PRIDE partner repository with the data set identifier PXD014137.

628 **SUPPLEMENTAL MATERIAL**

Supplemental Table S1: List of proteins identified and quantified in Col-0 and *bou-2* plants expressing the 3×HA-sGFP-TOM5 protein.

Supplemental Table S2: List of raw intensities and reliability of all quantified peptides.

Supplemental Figure S1: Schematic representation of the vector used to label mitochondria with triple HA-tag.

Supplemental Figure S2: Activity of malate dehydrogenase (MDH) in mitochondria rapidly isolated from 4-week-old Col-0 and *bou-2* leaves expressing the *UB10p-3×HA-sGFP-TOM5* construct.

ACKNOWLEDGEMENTS

This work was supported by the Deutsche Forschungsgemeinschaft (CRC 1208 and funding under Germany´s Excellence Strategy – EXC-2048/1 – project ID 390686111“).

FIGURE LEGENDS

Figure 1: Confocal microscopy of epitope-tagged mitochondria in leaf and root tissues of transgenic Arabidopsis Col-0 and *bou-2* lines expressing the *UB10p-3×HA-sGFP-TOM5* construct. (A–D) Images of transgenic Col-0 leaf (A) and root (B) tissues and transgenic *bou-2* leaf (C) and root (D) tissues expressing the 3×HA-sGFP-TOM5 protein. Green color represents GFP signal, whereas red color represents the signal of mitochondrial marker MitoTracker™ Red CMXRos. Bright field and merged images are shown in yellow. Scale bar = 10 µm.

Figure 2: Workflow showing the rapid isolation of epitope-tagged mitochondria via co-Immunopurification (co-IP) from Arabidopsis. Transgenic lines harboring the *UB10p-3×HA-sGFP-TOM5* construct and non-transgenic (control) plants were harvested and homogenized in a Warren blender. The extract was filtered and centrifuged to obtain a crude mitochondrial fraction. Epitope-tagged mitochondria were purified via co-IP using magnetic anti-HA beads. The purified mitochondria were washed and either lysed for immunoblot analysis or extracted for proteomics.

Figure 3: Immunoblot analysis of mitochondria isolated via co-IP or by differential centrifugation and gradient purification. Mitochondria were isolated from transgenic and non-transgenic (control) Col-0 and *bou-2* lines via co-IP using magnetic anti-HA beads (whole cell, Anti-HA IP) or using differential centrifugation and gradient purification (Extract, DC, Pur). Protein amounts were loaded as described in Material and Methods. Whole cell and extract samples were collected after tissue homogenization. Names of organelle marker

proteins are shown on the left side of the blots, and their subcellular localization is indicated on the right.

Figure 4: Latency of MDH activity in affinity-purified mitochondria. Mitochondria were rapidly isolated from transgenic and control Col-0 and *bou-2* plants via co-IP, with or without the addition of Triton X-114. The activity of MDH was calculated from the initial slope. Data represent mean ± SD of three replicates.

Figure 5: Characterization of enzyme activities in mitochondria isolated from 10-day-old transgenic Col-0 and *bou-2* lines grown at 3,000 ppm (HC) and after shift to 380 ppm (5d LC) via co-IP. (A) Malate dehydrogenase (MDH) activity. (B) Formate dehydrogenase (FDH) activity. (C) Aspartate aminotransferase (AspAT) activity. (D) γ-aminobutyric acid transaminase (GABA-T) activity. (E) Alanine aminotransferase (AlaAT) activity. (F) Glutamate dehydrogenase (GluDH) activity. Activities were calculated from initial slopes. Enzyme activities in transgenic Col-0 were set to 100%. Data represent mean ± SD of three biological replicates. Different letters indicate statistically significant differences between means for each enzyme ($P < 0.05$; one-way ANOVA).

SUPPLEMENTARY DATA

Supplemental Table S1: List of proteins identified and quantified in Col-0 and *bou-2* plants expressing the 3×HA-sGFP-TOM5 protein. Intensities of identified proteins are given as $\log_2$-transformed values. Subcellular localization was assigned using SUBA4. Difference between Col-0 and *bou-2* was calculated as the change in $\log_2$-transformed values. Significance was calculated using the Student *t*-test ($P < 0.05$).

Supplemental Table S2: List of raw intensities and reliability of all quantified peptides. PEP: Posterior Error Probability of identification.

Supplemental Figure S1: Schematic representation of the vector used to label mitochondria with triple HA-tag. The N-terminal end of Arabidopsis gene encoding the outer mitochondrial membrane protein TOM5 (At5g08040) was fused to the *synthetic green fluorescent protein* (*sGFP*) gene labeled with a triple hemagglutinin (3×HA) tag for co-Immunopurifiaction. The cassette was cloned into the pUTKan vector under the control of the Arabidopsis *UBIQUITIN10* promoter (*UB10p*) and stably introduced into Arabidopsis via the floral dip method.

Supplemental Figure S2: Activity of malate dehydrogenase (MDH) in mitochondria rapidly isolated from 4-week-old Col-0 and *bou-2* leaves expressing the *UB10p-3×HA-sGFP-TOM5* construct. MDH activity was measured as described in Material and Methods.

694 Activities were calculated from initial slopes. Enzyme activity in transgenic Col-0 was set to
695 100%. Data represent mean ± SD of three biological replicates. Asterisks indicate
696 statistically significant differences (***, $P < 0.001$; Student's *t*-test).

697

Table 1: List of significant differences in protein abundance between Col-0 *UB10p-3×HA-sGFP-TOM5* and *bou-2 UB10p-3×HA-sGFP-TOM5*. Difference was calculated as change of $\log_2$ of normalized intensity. List includes only proteins that show mitochondrial localization. List ranges from most downregulated in *bou-2 UB10p-3×HA-sGFP-TOM5* (top) to most upregulated *bou-2 UB10p-3×HA-sGFP-TOM5* (bottom). Significance was calculated with Student's t-test, $P < 0.05$.

AGI	Gene symbol	Gene description	Difference
AT5G46800	BOU	Mitochondrial substrate carrier family protein	-8,66407
AT2G42310	AT2G42310	ESSS subunit of NADH:ubiquinone oxidoreductase (complex I) protein	-2,0953
AT5G41685	AT5G41685	Mitochondrial outer membrane translocase complex, subunit Tom7	-1,90711
AT3G03100	AT3G03100	NADH:ubiquinone oxidoreductase, 17.2kDa subunit	-1,33356
AT5G53650	AT5G53650	ABC transporter A family protein	-1,25252
AT5G67590	FRO1	NADH-ubiquinone oxidoreductase-like protein	-1,0968
AT5G40810	AT5G40810	Cytochrome C1 family	-1,06444
AT3G27280	PHB4	prohibitin 4	-0,94888
AT3G27380	SDH2-1	succinate dehydrogenase 2-1	-0,764682
AT4G37660	AT4G37660	Ribosomal protein L12/ ATP-dependent Clp protease adaptor protein ClpS family protein	-0,732468
AT2G42210	OEP16-3	Mitochondrial import inner membrane translocase subunit Tim17/Tim22/Tim23 family protein	-0,710023
AT3G55400	OVA1	methionyl-tRNA synthetase / methionine-tRNA ligase / MetRS (cpMetRS)	-0,705525
AT5G14780	FDH	formate dehydrogenase	-0,697987

AT2G38670	PECT1	phosphorylethanolamine cytidylyltransferase 1	-0,606253
AT5G63400	ADK1	adenylate kinase 1	-0,603703
AT1G79230	MST1	mercaptopyruvate sulfurtransferase 1	-0,587758
AT4G30010	AT4G30010	ATP-dependent RNA helicase	-0,545131
AT3G03420	AT3G03420	Ku70-binding family protein	-0,531796
AT4G31810	AT4G31810	ATP-dependent caseinolytic (Clp) protease/crotonase family protein	-0,461768
AT1G19140	AT1G19140	ubiquinone biosynthesis COQ9-like protein	-0,455841
AT4G31460	AT4G31460	Ribosomal L28 family	-0,430804
AT1G54220	AT1G54220	Dihydrolipoamide acetyltransferase, long form protein	-0,324755
AT3G59820	LETM1	LETM1-like protein	0,42657
AT5G27540	MIRO1	MIRO-related GTP-ase 1	0,447933
AT3G10160	DFC	DHFS-FPGS homolog C	0,507662
AT1G71260	ATWHY2	WHIRLY 2	0,51931
AT5G15980	AT5G15980	Pentatricopeptide repeat (PPR) superfamily protein	0,8335

704

705

706 **Table 2: List of changes in protein abundance of glycine decarboxylase proteins,**
707 **serine hydroxymethyltransferase (SHM) and the enzymes malate dehydrogenase**
708 **(MDH), formate dehydrogenase (FDH), aspartate aminotransferase (ASP), γ-**
709 **aminobutyric acid transaminase (POP2), alanine aminotransferase (AlaAT) and**
710 **glutamate dehydrogenase (GDH).** Difference was calculated as change of log_2 of
711 normalized intensity. Significance was calculated with Student's t-test, $P < 0.05$.

712

AGI	Gene symbol	Gene description	Difference	Significant
AT4G33010	GLDP1	glycine decarboxylase P-protein 1	-0,373902	no
AT2G26080	GLDP2	glycine decarboxylase P-protein 2	-0,155379	no
AT2G35370	GDCH1	glycine decarboxylase H-protein 1	-0,760396	no
AT1G32470	GDCH3	glycine decarboxylase H-protein 3	0,173202	no
AT1G11860	GLDT	Glycine cleavage T-protein family	-0,164196	no
AT1G48030	GDCL1	mitochondrial lipoamide dehydrogenase 1	-0,0284281	no
AT3G17240	GDCL2	mitochondrial lipoamide dehydrogenase 2	-0,217162	no
AT4G37930	SHM1	serine hydroxymethyltransferase 1	0,109162	no
AT5G26780	SHM2	serine hydroxymethyltransferase 2	0,696879	no
AT5G14780	FDH	formate dehydrogenase	-0,697987	yes
AT5G18170	GDH1	glutamate dehydrogenase 1	0,91113	no
AT5G07440	GDH2	glutamate dehydrogenase 2	0,105005	no
AT3G22200	POP2	γ-aminobutyric acid transaminase	0,345683	no
AT1G17290	AlaAT1	alanine aminotransferase 1	0,640894	no
AT1G72330	AlaAT2	alanine aminotransferase 2	0,223008	no

AT2G30970	ASP1	aspartate aminotransferase 1	0,399954	no
AT1G53240	mMDH1	Lactate/malate dehydrogenase family protein	0,564951	no
AT3G15020	mMDH2	Lactate/malate dehydrogenase family protein	0,0343099	no

713

714

Parsed Citations

Chen WW, Freinkman E, Wang T, Birsoy K, Sabatini DM (2016) Absolute Quantification of matrix metabolites reveals the dynamics of mitochondrial metabolism. Cell 166: 1324-1337.e11
Pubmed: Author and Title
Google Scholar: Author Only Title Only Author and Title

Clark SM, Di Leo R, Dhanoa PK, Van Cauwenberghe OR, Mullen RT, Shelp BJ (2009) Biochemical characterization, mitochondrial localization, expression, and potential functions for an Arabidopsis gamma-aminobutyrate transaminase that utilizes both pyruvate and glyoxylate. J Exp Bot 60: 1743–57
Pubmed: Author and Title
Google Scholar: Author Only Title Only Author and Title

Clough SJ, Bent AF (1998) Floral dip: a simplified method for Agrobacterium-mediated transformation of Arabidopsis thaliana. Plant J 16: 735–43
Pubmed: Author and Title
Google Scholar: Author Only Title Only Author and Title

De Col V, Fuchs P, Nietzel T, Elsässer M, Voon CP, Candeo A, Seeliger I, Fricker MD, Grefen C, Møller IM, et al (2017) ATP sensing in living plant cells reveals tissue gradients and stress dynamics of energy physiology. Elife 6: 1–29
Pubmed: Author and Title
Google Scholar: Author Only Title Only Author and Title

Collakova E, Goyer A, Naponelli V, Krassovskaya I, Gregory JF, Hanson AD, Shachar-Hill Y (2008) Arabidopsis 10-formyl tetrahydrofolate deformylases are essential for photorespiration. Plant Cell 20: 1818–32
Pubmed: Author and Title
Google Scholar: Author Only Title Only Author and Title

Dietmeier K, Hönlinger A, Bömer U, Dekker PJ, Eckerskorn C, Lottspeich F, Kubrich M, Pfanner N (1997) Tom5 functionally links mitochondrial preprotein receptors to the general import pore. Nature 388: 195–200
Pubmed: Author and Title
Google Scholar: Author Only Title Only Author and Title

Eisenhut M, Planchais S, Cabassa C, Guivarc'H A, Justin AM, Taconnat L, Renou JP, Linka M, Gagneul D, Timm S, et al (2013) Arabidopsis A BOUT de SOUFFLE is a putative mitochondrial transporter involved in photorespiratory metabolism and is required for meristem growth at ambient CO2 levels. Plant J 73: 836–849
Pubmed: Author and Title
Google Scholar: Author Only Title Only Author and Title

Eisenhut M, Roell M, Weber APM (2019) Mechanistic understanding of photorespiration paves the way to a new green revolution. New Phytol doi: 10.1111/nph.15872
Pubmed: Author and Title
Google Scholar: Author Only Title Only Author and Title

Engel N, van den Daele K, Kolukisaoglu U, Morgenthal K, Weckwerth W, Parnik T, Keerberg O, Bauwe H (2007) Deletion of Glycine Decarboxylase in Arabidopsis Is Lethal under Nonphotorespiratory Conditions. Plant Physiol 144: 1328–1335
Pubmed: Author and Title
Google Scholar: Author Only Title Only Author and Title

Fromm S, Senkler J, Eubel H, Peterhänsel C, Braun H-P (2016) Life without complex I: proteome analyses of an Arabidopsis mutant lacking the mitochondrial NADH dehydrogenase complex. J Exp Bot 67: 3079–93
Pubmed: Author and Title
Google Scholar: Author Only Title Only Author and Title

Hanson AD, Gregory JF (2011) Folate biosynthesis, turnover, and transport in plants. Annu Rev Plant Biol 62: 105–125
Pubmed: Author and Title
Google Scholar: Author Only Title Only Author and Title

Hooper CM, Castleden IR, Tanz SK, Aryamanesh N, Millar AH (2017) SUBA4: the interactive data analysis centre for Arabidopsis subcellular protein locations. Nucleic Acids Res 45: D1064–D1074
Pubmed: Author and Title
Google Scholar: Author Only Title Only Author and Title

Horie C, Suzuki H, Sakaguchi M, Mihara K (2003) Targeting and assembly of mitochondrial tail-anchored protein Tom5 to the TOM complex depend on a signal distinct from that of tail-anchored proteins dispersed in the membrane. J Biol Chem 278: 41462–41471
Pubmed: Author and Title
Google Scholar: Author Only Title Only Author and Title

Hu Y, Zou W, Wang Z, Zhang Y, Hu Y, Qian J, Wu X, Ren Y, Zhao J (2019) Translocase of the outer mitochondrial membrane 40 is required for mitochondrial biogenesis and embryo development in Arabidopsis. Front Plant Sci 10: 1–17
Pubmed: Author and Title
Google Scholar: Author Only Title Only Author and Title

Husic DW, Husic HD, Tolbert NE, Black CC (1987) The oxidative photosynthetic carbon cycle or C2 cycle. CRC Crit Rev Plant Sci 5: 45–

Pubmed: Author and Title
Google Scholar: Author Only Title Only Author and Title

Keech O, Dizengremel P, Gardeström P (2005) Preparation of leaf mitochondria from Arabidopsis thaliana. Physiol Plant. doi: 10.1111/j.1399-3054.2005.00521.x

Pubmed: Author and Title
Google Scholar: Author Only Title Only Author and Title

Kelly GJ, Latzko E (1976) Inhibition of spinach-leaf phosphofructokinase by 2-phosphoglycollate. FEBS Lett 68: 55–58

Pubmed: Author and Title
Google Scholar: Author Only Title Only Author and Title

Kleinboelting N, Huep G, Kloetgen A, Viehoever P, Weisshaar B (2012) GABI-Kat SimpleSearch: new features of the Arabidopsis thaliana T-DNA mutant database. Nucleic Acids Res 40: D1211–D1215

Pubmed: Author and Title
Google Scholar: Author Only Title Only Author and Title

Klodmann J, Senkler M, Rode C, Braun H-P (2011) Defining the protein complex proteome of plant mitochondria. Plant Physiol 157: 587–598

Pubmed: Author and Title
Google Scholar: Author Only Title Only Author and Title

Kolli R, Soll J, Carrie C (2019) OXA2b is crucial for proper membrane insertion of COX2 during biogenesis of Complex IV in plant mitochondria. Plant Physiol 179: 601–615

Pubmed: Author and Title
Google Scholar: Author Only Title Only Author and Title

König AC, Hartl M, Boersema PJ, Mann M, Finkemeier I (2014) The mitochondrial lysine acetylome of Arabidopsis. Mitochondrion 19: 252–260

Pubmed: Author and Title
Google Scholar: Author Only Title Only Author and Title

Kühn K, Obata T, Feher K, Bock R, Fernie AR, Meyer EH (2015) Complete mitochondrial Complex I deficiency induces an up-regulation of respiratory fluxes that is abolished by traces of functional Complex I. Plant Physiol 168: 1537–1549

Pubmed: Author and Title
Google Scholar: Author Only Title Only Author and Title

van der Laan M, Horvath SE, Pfanner N (2016) Mitochondrial contact site and cristae organizing system. Curr Opin Cell Biol 41: 33–42

Pubmed: Author and Title
Google Scholar: Author Only Title Only Author and Title

Laemmli UK (1970) Cleavage of structural proteins during the assembly of the head of bacteriophage T4. Nature 227: 680

Pubmed: Author and Title
Google Scholar: Author Only Title Only Author and Title

Lawand S, Dorne A-J, Long D, Coupland G, Mache R, Carol P (2002) Arabidopsis ABOUT DE SOUFFLE, which is homologous with mammalian carnitine acyl carrier, is required for postembryonic growth in the light. Plant Cell 14: 2161–2173

Pubmed: Author and Title
Google Scholar: Author Only Title Only Author and Title

Linka M, Weber APM (2005) Shuffling ammonia between mitochondria and plastids during photorespiration. Trends Plant Sci 10: 461–5

Pubmed: Author and Title
Google Scholar: Author Only Title Only Author and Title

Mansilla N, Racca S, Gras DE, Gonzalez DH, Welchen E (2018) The Complexity of Mitochondrial Complex IV: An update of cytochrome c oxidase biogenesis in plants. Int J Mol Sci 19: 1–34

Pubmed: Author and Title
Google Scholar: Author Only Title Only Author and Title

Meyer EH, Welchen E, Carrie C (2019) Assembly of the complexes of the oxidative phosphorylation system in land plant mitochondria. Annu Rev Plant Biol 70: 23–50

Pubmed: Author and Title
Google Scholar: Author Only Title Only Author and Title

Millar AH, Eubel H, Jänsch L, Kruft V, Heazlewood JL, Braun H-P (2004) Mitochondrial cytochrome c oxidase and succinate dehydrogenase complexes contain plant specific subunits. Plant Mol Biol 56: 77–90

Pubmed: Author and Title
Google Scholar: Author Only Title Only Author and Title

Millar AH, Sweetlove LJ, Giegé P, Leaver CJ (2001) Analysis of the Arabidopsis mitochondrial proteome. Plant Physiol 127: 1711–27

Pubmed: Author and Title
Google Scholar: Author Only Title Only Author and Title

Miyashita Y, Dolferus R, Ismond KP, Good AG (2007) Alanine aminotransferase catalyses the breakdown of alanine after hypoxia in

Arabidopsis thaliana. Plant J 49: 1108–1121
Pubmed: Author and Title
Google Scholar: Author Only Title Only Author and Title

Monné M, Daddabbo L, Gagneul D, Obata T, Hielscher B, Palmieri L, Miniero DV, Fernie AR, Weber APM, Palmieri F (2018) Uncoupling proteins 1 and 2 (UCP1 and UCP2) from Arabidopsis thaliana are mitochondrial transporters of aspartate, glutamate, and dicarboxylates. J Biol Chem 293: 4213–4227
Pubmed: Author and Title
Google Scholar: Author Only Title Only Author and Title

Murcha MW, Kmiec B, Kubiszewski-Jakubiak S, Teixeira PF, Glaser E, Whelan J (2014) Protein import into plant mitochondria: Signals, machinery, processing, and regulation. J Exp Bot 65: 6301–6335
Pubmed: Author and Title
Google Scholar: Author Only Title Only Author and Title

Murcha MW, Narsai R, Devenish J, Kubiszewski-Jakubiak S, Whelan J (2015) MPIC: A mitochondrial protein import components database for plant and non-plant species. Plant Cell Physiol 56: e10
Pubmed: Author and Title
Google Scholar: Author Only Title Only Author and Title

Nickel C, Horneff R, Heermann R, Neumann B, Jung K, Soll J, Schwenkert S (2019) Phosphorylation of the outer membrane mitochondrial protein OM64 influences protein import into mitochondria. Mitochondrion 44: 93–102
Pubmed: Author and Title
Google Scholar: Author Only Title Only Author and Title

Ogren WL, Bowes G (1971) Ribulose diphosphate carboxylase regulates soybean photorespiration. Nat New Biol 230: 159
Pubmed: Author and Title
Google Scholar: Author Only Title Only Author and Title

Oliver DJ, Neuburger M, Bourguignon J, Douce R (1990) Interaction between the component enzymes of the glycine decarboxylase multienzyme complex. Plant Physiol 94: 833–9
Pubmed: Author and Title
Google Scholar: Author Only Title Only Author and Title

Pendergrass W, Wolf N, Pool M (2004) Efficacy of MitoTracker GreenTM and CMXRosamine to measure changes in mitochondrial membrane potentials in living cells and tissues. Cytom Part A 61: 162–169
Pubmed: Author and Title
Google Scholar: Author Only Title Only Author and Title

Peterhansel C, Horst I, Niessen M, Blume C, Kebeish R, Kürkcüoglu S, Kreuzaler F (2010) Photorespiration. Arab B 8: e0130
Pubmed: Author and Title
Google Scholar: Author Only Title Only Author and Title

Peters K, Belt K, Braun H-P (2013) 3D gel map of Arabidopsis Complex I. Front Plant Sci 4: 1–9
Pubmed: Author and Title
Google Scholar: Author Only Title Only Author and Title

Porcelli V, Vozza A, Calcagnile V, Gorgoglione R, Arrigoni R, Fontanesi F, Marobbio CMT, Castegna A, Palmieri F, Palmieri L (2018) Molecular identification and functional characterization of a novel glutamate transporter in yeast and plant mitochondria. Biochim Biophys Acta - Bioenerg 1859: 1249–1258
Pubmed: Author and Title
Google Scholar: Author Only Title Only Author and Title

Rao RSP, Salvato F, Thal B, Eubel H, Thelen JJ, Møller IM (2017) The proteome of higher plant mitochondria. Mitochondrion 33: 22–37
Pubmed: Author and Title
Google Scholar: Author Only Title Only Author and Title

Schneider M, Knuesting J, Birkholz O, Heinisch JJ, Scheibe R (2018) Cytosolic GAPDH as a redox-dependent regulator of energy metabolism. BMC Plant Biol 18: 1–14
Pubmed: Author and Title
Google Scholar: Author Only Title Only Author and Title

Schürholz A-K, López-Salmerón V, Li Z, Forner J, Wenzl C, Gaillochet C, Augustin S, Barro AV, Fuchs M, Gebert M, et al (2018) A Comprehensive toolkit for inducible, cell type-specific gene expression in Arabidopsis. Plant Physiol 178: 40–53
Pubmed: Author and Title
Google Scholar: Author Only Title Only Author and Title

Senkler J, Senkler M, Eubel H, Hildebrandt T, Lengwenus C, Schertl P, Schwarzländer M, Wagner S, Wittig I, Braun HP (2017) The mitochondrial complexome of Arabidopsis thaliana. Plant J 89: 1079–1092
Pubmed: Author and Title
Google Scholar: Author Only Title Only Author and Title

Suh JR, Herbig AK, Stover PJ (2001) New perspectives on folate catabolism. Annu Rev Nutr 21: 255–82
Pubmed: Author and Title
Google Scholar: Author Only Title Only Author and Title

Sunderhaus S, Klodmann J, Perales M, Jänsch L, Dudkina N V., Braun H-P, Heinemeyer J, Boekema EJ, Zabaleta E (2006) Carbonic anhydrase subunits form a matrix-exposed domain attached to the membrane arm of mitochondrial Complex I in plants. J Biol Chem 281: 6482–6488

Pubmed: Author and Title
Google Scholar: Author Only Title Only Author and Title

Sweetlove LJ, Taylor NL, Leaver CJ (2007) Isolation of intact, functional mitochondria from the model plant Arabidopsis thaliana. From Methods Mol Biol 372: 125–136

Pubmed: Author and Title
Google Scholar: Author Only Title Only Author and Title

Tomaz T, Lee CP, Bagard M, Pracharoenwattana I, Linde P, Smith SM, Gardestro P, Millar AH, Carroll AJ, Stro E, et al (2010) Mitochondrial malate dehydrogenase lowers leaf respiration and alters photorespiration and plant growth in Arabidopsis. Plant Physiol 154: 1143–1157

Pubmed: Author and Title
Google Scholar: Author Only Title Only Author and Title

Turano FJ, Dashner R, Upadhyaya A, Caldwell C (1996) Purfication of mitochondrial glutamate dehydrogenase from dark-grown soybean seedlings. Plant Physiol 112: 1357–1364

Pubmed: Author and Title
Google Scholar: Author Only Title Only Author and Title

Voll LM, Jamai A, Renné P, Voll H, McClung CR, Weber APM (2006) The photorespiratory Arabidopsis shm1 mutant is deficient in SHM1. Plant Physiol 140: 59–66

Pubmed: Author and Title
Google Scholar: Author Only Title Only Author and Title

Werhahn W, Jänsch L, Braun HP (2003) Identification of novel subunits of the TOM complex from Arabidopsis thaliana. Plant Physiol Biochem 41: 407–416

Pubmed: Author and Title
Google Scholar: Author Only Title Only Author and Title

Werhahn W, Niemeyer A, Jänsch L, Kruft V, Schmitz UK, Braun H (2001) Purification and characterization of the preprotein translocase of the outer mitochondrial membrane from Arabidopsis. Identification of multiple forms of TOM20. Plant Physiol 125: 943–54

Pubmed: Author and Title
Google Scholar: Author Only Title Only Author and Title

Wiedemann N, Frazier AE, Pfanner N (2004) The protein import machinery of mitochondria. J Biol Chem 279: 14473–6

Pubmed: Author and Title
Google Scholar: Author Only Title Only Author and Title

Wilkie SE, Warren MJ (1998) Recombinant expression, purification, and characterization of three isoenzymes of aspartate aminotransferase from Arabidopsis thaliana. Protein Expr Purif 12: 381–389

Pubmed: Author and Title
Google Scholar: Author Only Title Only Author and Title

Yang Y, Costa A, Leonhardt N, Siegel RS, Schroeder JI (2008) Isolation of a strong Arabidopsis guard cell promoter and its potential as a research tool. Plant Methods 4: 1–15

Pubmed: Author and Title
Google Scholar: Author Only Title Only Author and Title